Journal of Alloys and Compounds 702 (2017) 538–545

Contents lists available at ScienceDirect

Journal of Alloys and Compounds

journal homepage: http://www.elsevier.com/locate/jalcom

Effect of hafnium addition on the microstructure and tensile properties of aluminum added high-Cr ODS steels

Hongqing Dong [a], Liming Yu [a, *], Yongchang Liu [a], Chenxi Liu [a], Huijun Li [a], Jiefeng Wu [b]

[a] State Key Lab of Hydraulic Engineering Simulation and Safety, Tianjin Key Lab of Composite and Functional Materials, Tianjin University, Tianjin, 300072, China
[b] Institute of Plasma Physics, Chinese Academy of Sciences, Hefei, 230031, China

ARTICLE INFO

Article history:
Received 6 October 2016
Received in revised form
3 January 2017
Accepted 26 January 2017
Available online 27 January 2017

Keywords:
Hf addition
ODS steel
Grain size
Oxide particles
Tensile

ABSTRACT

To investigate the effects of hafnium (Hf) addition on the microstructural and mechanical performance of an aluminum (Al) added 16Cr ODS steel, the microstructures of the 16Cr ODS steel with and without Hf were investigated by EBSD and TEM, and tensile tests were conducted at high temperature to evaluate the strength and ductility changes at different temperatures. The Hf addition is beneficial to the grain refinement of the 16Cr ODS steel. The average grain size decreases from 1.795 μm to 1.027 μm with Hf addition. In addition to the Y–Al–O nanoparticles, Y–Hf–O complex oxides with a finer size are also observed in the sample with the Hf addition, which reduces the mean size of oxides within the steel and increases the number density of the oxide particles. The yield strength and tensile strength of the 16Cr ODS steel are further improved by Hf addition due to its optimized microstructures with further refined grains.

1. Introduction

Due to excellent high-temperature strength and superior radiation resistance, oxide dispersion strengthened (ODS) steels have been considered as candidate materials for structural components in the future fission and fusion reactor [1–3]. Outstanding oxidation and corrosion resistance are required for ODS steels used in a fission power plant due to their long continuous operating time. Al has been regarded as one of the significant element in improving the corrosion resistance of ODS steels due to the formation of dense alumina layer on the surface [4]. Thus, different type of Fe–Cr–Al ODS steels have been developed including commercial alloys such as PM2000 (20 wt% Cr and 5.5 wt% Al) and MA956 (20 wt% Cr and 4.5 wt% Al). It has been proved that Fe–Cr–Al ODS steels possessed superior corrosion resistance. For example, Lim et al. have researched the corrosion behaviors of PM2000 and MA956 in stagnant lead-bismuth eutectic (LBE) at 500 °C and 550 °C for 500 h and observed only relatively thin continuous Al_2O_3 layers on the surface but no LBE penetration into the metal [5,6].

As widely described, the formation of dispersed oxide particles within matrix would go through two stages, oxides (i.e. Y_2O_3) decompose and dissolve in matrix during ball milling and then re-precipitate during the subsequent consolidation. However, the presence of Al would coarsen the dispersed oxide particles by combining with Y, O atoms to form Y–Al–O particles instead of Y_2O_3 nanoparticles, which would deteriorate the high-temperature strength of ODS steels [7]. In recent years, many researchers found that the addition of Zr to Al-containing ODS steels could promote the formation of finer Y–Zr–O nanoparticles, which had higher bonding energy than coarse Y–Al–O particles. As a result, finer Y–Zr–O particles could improve the high-temperature performance of Al-containing ODS steels and maintain the corrosion resistance simultaneously [8]. Kimura et al. found that small addition of Zr to Al-added ODS steels could significantly increase the creep strength at 973 K, and the high temperature compatibility with LBE could be effectively improved [9,10]. Hf, belonging to the IVB group as Zr element, also has a more negative oxide formation energy than that of Al element [10]. Therefore, it is expected that the addition of Hf would promote the formation of finer Y–Hf–O phases instead of Y–Al–O phases and increase the number density of oxide particles. The presence of Hf is inclined to form compounds with high melting points and stable thermodynamic properties. This feature is attractive to those components especially required to serve in high temperature environment for a long time. To some extent, Hf is helpful to improve the corrosion resistance [11].

* Corresponding author.
E-mail address: lmyu@tju.edu.cn (L. Yu).

http://dx.doi.org/10.1016/j.jallcom.2017.01.298
0925-8388/

In this work, the effect of Hf addition on the microstructure and tensile properties of an Al-added high-Cr ODS steel (16Cr ODS) prepared by high-energy ball milling and HIPing was investigated. The grain size and its distribution were investigated using EBSD. The dispersion morphology and crystal structures of oxide particles were studied by TEM and HRTEM. In addition, tensile properties at different testing temperatures were measured and discussed in detail.

2. Experimental

Powders of Fe16Cr3Al-1.5W-0.35Y_2O_3 (16Cr ODS) were prepared using mechanical alloying of the argon-gas atomized Fe16Cr3Al-1.5W (wt.%) pre-alloyed powders (average size 50 μm) mixed with 0.35 wt% Y_2O_3 (40 nm) particles in high purity argon atmosphere. The contents of impurity elements O, C, N were strictly controlled during the preparation of pre-alloyed powders. The ball milling process was carried out in a high-performance planetary ball mill (QM-2SP12, Nanjing NanDa Instrument Plant, China) with stainless steel containers (2000 ml) and a combination of 6 mm (80 wt%) and 10 mm (20 wt%) diameter steel balls at the rotating speed of 250 rpm for 30 h, and the weight ratio of ball to powder was 10:1. The as-milled powders were then sealed in mild-steel cans and degassed at 450 °C until 0.002 Pa vacuum was achieved, and then consolidated by hot isostatic pressing (HIP) at 1150 °C for 3 h under a pressure of 150 MPa. The fabrication process of the Hf added Fe16Cr3Al-1.5W-0.5Hf-0.35Y_2O_3 (16Cr-0.5Hf ODS) was the same as described above. Hf was added as elemental powders (purity 99.9%, mean size 10 μm) before milling.

The actual densities of HIPed specimens were measured by means of the Archimedes method, while the theoretical values calculated were 7.41 g/cm^3 and 7.42 g/cm^3 for 16Cr ODS and 16Cr-0.5Hf ODS, respectively. After calculation, the relative densities of ODS samples with and without Hf which can be expressed by the ratio of the actual density to the theoretical value were 96.1% and 98.6%.

The grain size and distribution of two ODS steels were observed and measured by Hitachi S3400 scanning electron microscopy (SEM) equipped with Oxford instruments electron backscatter diffraction (EBSD), and the crystal structure and distribution were investigated by transmission electron microscopy (TEM, JEM-2100f, JEOL, Japan). EBSD specimens were prepared by a standard metallographic preparation method, followed by Ar^+-ion polishing (RES101, Leica, Germany) to remove surface stress layer. Results were analyzed using the HKL channel 5 software. TEM specimens were prepared by mechanical grinding to about 50 μm thickness and then punched into 3 mm TEM discs. The TEM discs were etched by a twin-jet electro-polishing machine using 5% perchloric acid and 95% ethanol polishing solution at −20 °C.

Tensile tests were carried out using a universal electronic material testing machine (Z330, Zwick/Roell, Germany) with extensometer in air at four different temperatures (room temperature (RT), 400, 600, 800 °C) with a nominal strain rate of 7×10^{-4} s^{-1}. The rod shaped specimens for tensile test were cut from the as-HIPed products with a gauge length of 25 mm and a diameter of 5 mm.

3. Results and discussion

3.1. Microstructure of ODS steels matrix

Fig. 1 (a) and (b) show the microstructures of 16Cr ODS and 16Cr-0.5Hf ODS steels matrix, respectively. The matrix microstructures of two ODS steels consist of similar equiaxed ferrite grains which exhibit hexagonal structure with different sizes. As it will be shown in the EBSD study later, the sizes of some coarse grains in 16Cr ODS steel are in a scale of a few micrometers while some fine grains are hundreds of nanometers. On the other hand, the grain sizes of the ODS sample containing Hf distribute from 500 nm to 4 μm. Generally, the 16Cr-0.5Hf ODS steel have smaller grain size than the material without Hf addition. The main reasons for this significant difference in grain size are the incomplete recrystallization and non-uniform grain growth during the densification process [12,13]. However, for the enhancement of contrast in this diffraction mode, a small number of dislocations can be found in grains. It can also be seen from Fig. 1 that oxide particles with different sizes are distributed homogeneously along the grain boundaries as well as in the grains. These particles pin on grain boundaries and dislocations and then hinder the movement of them, which correspond to Hall-Petch and Orowan strengthening mechanism, respectively [14–16]. As a result, the mechanical strength can be significantly enhanced due to the limited grain growth and dislocation movement.

3.2. Distribution and structure characterization of oxide particles

The TEM bright field micrographs of oxide particles and the corresponding histograms of oxide particles distribution in both ODS steels are illustrated in Fig. 2 (a) and (b). The histograms of oxide particles size distribution are obtained by counting more than 350 particles from different TEM regions. Oxide particles distribute homogeneously in the grains with sizes varying from a few nanometers to tens of nanometers. Almost all of the oxide particles exhibit spherical shape in dark contrast at this diffraction condition. It is observed from Fig. 2 (a) and (b) that the oxide

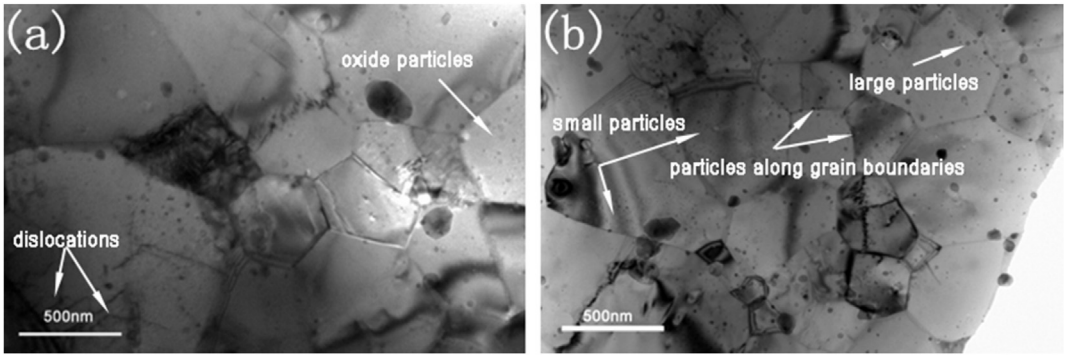

Fig. 1. BFTEM images of matrix microstructure of (a) 16Cr ODS steel (b) 16Cr-0.5Hf ODS steel.

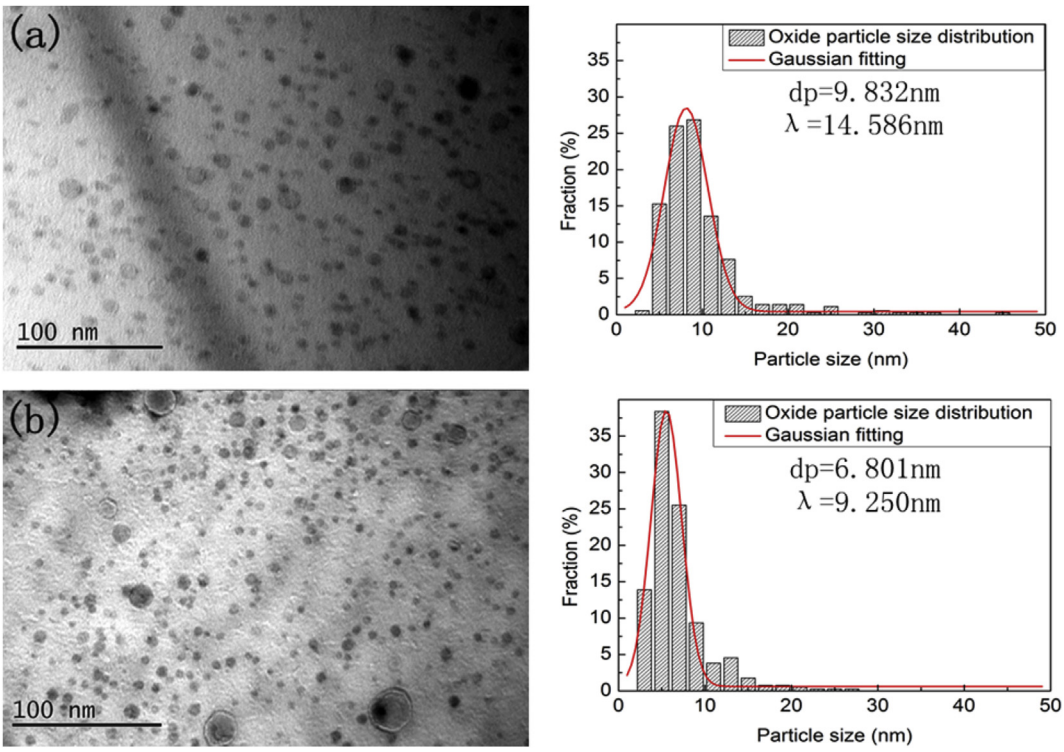

Fig. 2. BFTEM images and corresponding histograms of oxide particles distribution within (a) 16Cr ODS (b) 16Cr-0.5Hf ODS steels.

particles size and the inter-particle spacing become smaller, while the number density increases obviously with 0.5 wt% Hf addition. The statistical results of mean particle diameters, average inter-particle distances, number densities of particles counted from TEM micrographs are summarized in Table 1. It can be seen from Table 1 that the mean size of oxide particles decreases from 9.832 nm to 6.801 nm and the mean inter-particle distance decreases from 14.586 nm to 9.250 nm when Hf is added. Meanwhile, the number density of particles changes from 2.1×10^{23} m^{-3} to 3.7×10^{23} m^{-3} with Hf addition. The particle size distribution of the 16Cr ODS steel is broad with a size varying from a minimum size of 2.92 nm to a maximum size of more than 40 nm, while the size of most particles in the Hf-added sample is less than 10 nm. Furthermore, the fraction of oxide particles smaller than 5 nm for the 16Cr-0.5Hf ODS is almost five times more than that in the ODS steels without Hf. These results demonstrate that adding Hf to the Al-containing high-Cr ODS steels can further refine the oxide particles size and increase the number density of oxide particles.

The change in the particle distribution in the ODS steel with Hf addition may be due to the transformation in the crystal structures of the oxide particles. Therefore, it is necessary to characterize the crystal structures of oxides.

Fig. 3 (a)–(d) shows HRTEM images of two different oxide particles randomly selected in 16Cr ODS steel, combining with the corresponding fast Fourier transformation (FFT) images. According to the calibration of the FFT image shown in Fig. 3 (b), the particle with an 8 nm diameter presented in Fig. 3 (a) is $YAlO_3$ perovskite (YAP) structure, which is oriented with a [210] crystal zone axis. Three spots marked by circles represent three atomic planes $(1\,\bar{2}\,1)$, (002), $(\bar{1}\,21)$ with spacing 0.25 nm, 0.26 nm, 0.26 nm, respectively. The angle between each two adjacent planes is 59.66°. The particle presented in Fig. 3 (c) shows a different crystal structure. Here the particle of 15 nm diameter is oriented with a [010] zone axis. The angle is 32.47° between planes (402) and (305) and 49.4° between planes (305) and $(\bar{1}\,03)$. The interplanar spacing between these adjacent planes are 0.26 nm, 0.21 nm, 0.38 nm, respectively, which corresponds to $Y_3Al_5O_{12}$ garnet (YAG) structure [17,18]. Although the crystal structures of oxides are different, it can be concluded that the oxide particles within the 16Cr ODS matrix are all Y–Al–O phase.

Table 1
Mean particle diameters and particle radii, average inter-particle distances, number densities of particles of two ODS steels counted from TEM micrographs.

	d_p (nm)	r_p (nm)	λ (nm)	n_v (m^{-3})
16Cr ODS	9.832	4.916	14.586	2.1×10^{23}
16Cr-0.5Hf ODS	6.801	3.401	9.250	3.7×10^{23}

The HRTEM image and the corresponding FFT image of oxide particles randomly selected in the 16Cr-0.5Hf ODS steel are presented in Fig. 4 (a)–(d). The crystal structures change is evident from the display of FFT images compared with Fig. 3 (b) and (d). Fig. 4 (a) shows an 8 nm diameter oxide particle surrounded by ferrite matrix, and the corresponding FFT image is presented in Fig. 4 (b). The plane spacing measured from relevant spots distances in three directions are 0.29 nm, 0.19 nm and 0.30 nm, respectively, which correspond to $d_{Y2Hf2O7(111)}$ (0.30 nm), $d_{Y2Hf2O7(202)}$ (0.18 nm) and $d_{Y2Hf2O7(1\,\bar{1}\,1)}$ (0.30 nm). Thus, the presence of $Y_2Hf_2O_7$ is confirmed, which also indicates the addition of Hf can promote the formation of Y–Hf–O particles. In addition, there is also a Y–Al–O phase as a larger particle shown in Fig. 4 (c). The measured plane distance is 0.38 nm, which corresponds to the (220) plane of monoclinic $Y_4Al_2O_9$ (YAM). The formation of $Y_2Hf_2O_7$ may partly replace the Y–Al–O particles, and the coexistence of both particles may be due to the insufficient content of Hf element, which allows the large amount of Al atoms to have more opportunities to form Y–Al–O particles.

The precipitation of oxides is accomplished through nucleation and growth. It is considered that oxide crystals nucleate on a particular lattice plane of the ferrite matrix and the interfaces

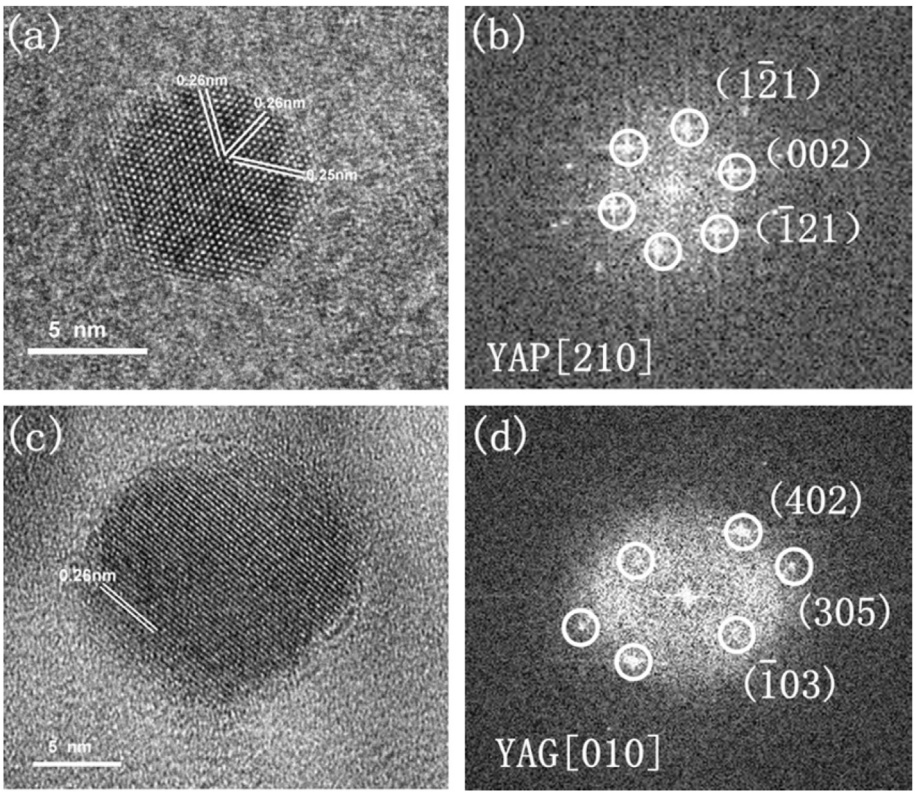

Fig. 3. HRTEM micrographs (a, b) and corresponding FFT image (c, d) of oxide particles in 16Cr ODS steel.

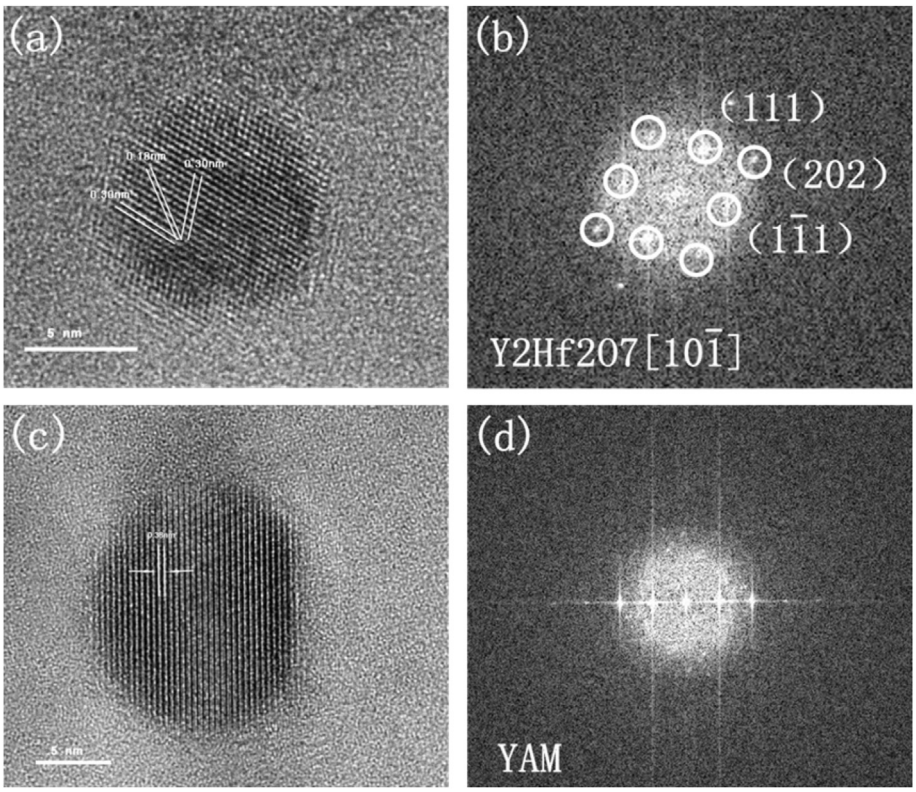

Fig. 4. HRTEM micrographs (a, b) and corresponding FFT image (c, d) of oxide particles in 16Cr-0.5Hf ODS steel.

between the particle and the matrix grow through the surface diffusion with the minimum surface energy. Under the effect of surface tension, atomic planes stacking leads to the formation of spherical or faceted particles. According to Figs. 3 and 4, the interfaces between the particles and the matrix in both alloys are partially coherent. The formation of coherent or partially coherent interfaces can lower the energy barrier for nucleation and reduce the interfacial energy, which is beneficial to increasing the nucleation and inhibiting the growth of oxides [19–21]. Additionally, there is a strong affinity of Hf atoms with oxygen, meanwhile, both reactive metal species Y and Hf have limited diffusion coefficient and solubility in the α-(Fe, Cr) matrix. Hf and O atoms bond with each other which is beneficial to prevent the coarsening of oxides [19,23]. Y–Hf–O clusters have lower Gibbs energy than Y–Al–O clusters in the Fe matrix, which indicates that adding Hf to Al-containing ODS steels can promote the formation of Y–Hf–O particles with higher stability instead of Y–Al–O particles [22–24]. Therefore, the growth rate of oxides was restricted effectively and the small size of particles can be maintained well at high temperature. From the above, the formation of Y–Hf–O particles may be the direct reason for the refinement and homogenization of oxide particles. Furthermore, the uniform distribution of fine particles is very beneficial to the mechanical properties improvement of ODS steels.

3.3. EBSD analysis of grain size and distribution

The EBSD grain orientation maps (inverse pole figure X, IPFX) for 16Cr ODS and 16Cr-0.5Hf ODS steels are shown in Fig. 5. Each different color in IPF maps represents a different crystallographic orientation in the standard triangle [25,26]. The grains for both ODS steels show a random orientation. The microstructures of both ODS steels exhibit equiaxed ferrite grains and display heterogeneous grain size distribution for the irregular assembly of large grains, surrounded by relatively small grains. The diameters of large particles reach dozens of times larger than that of small particles. Furthermore, notable changes in the grain size and distribution can be observed with Hf addition. As shown in Fig. 5 (a) with (b), the mean grain size for the ODS sample with Hf addition is smaller than the ODS without Hf addition and its grains are also distributed more uniformly. The statistical analysis results on the grain size distribution for both ODS steels are shown in Fig. 6. It can be found that the average grain size of 16Cr ODS steel is 1.795 μm and almost all grains have grain sizes greater than 1 μm, while the mean size of ODS steel containing Hf is only 1.027 μm and more than 60% of grains have grain sizes in hundreds of nanometers. It can be concluded from the above results and analysis that the addition of Hf to 16Cr ODS steel has a notable influence on the refinement of grain size.

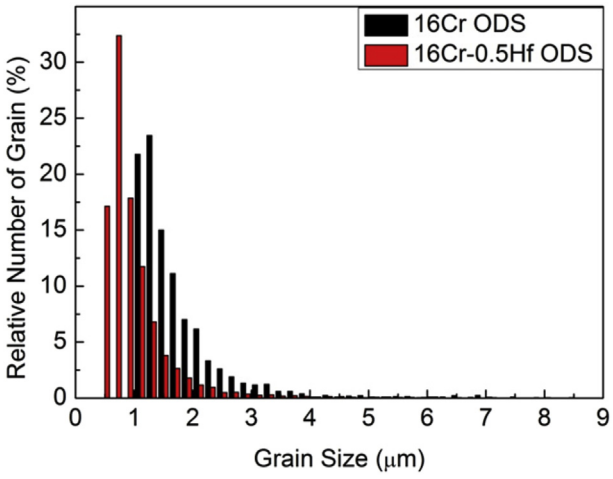

Fig. 6. Statistical figure on grain size distribution of two ODS steels.

The changes of grain size and distribution after Hf addition are closely related to the changes of size and density of oxide particles precipitated in the grain boundaries. The ultimate grain size depends upon the effect of pinning particles which can be calculated by Zener-Smith equation [27]:

$$R = \frac{4r_p}{3f_v} \tag{1}$$

where R and r_p are the mean radii of the matrix grains and oxide dispersion particles, respectively and f_v is the volume fraction of oxides in Fe matrix. According to Eq. (1), the size of matrix grains decreases as the refinement of the oxide particles when volume fraction is kept as a constant. As discussed above, the addition of Hf element can further refine the grain size and increase the number density of oxide particles in the ODS matrix. Plenty of finer particles such as Y–Hf–O or Y–Al–O pinning on the grain boundaries can better prevent the migration of grain boundaries due to more energy required to overcome these obstacles, and thus hindering further grain growth more effectively at high temperature [28]. Consequently, the grain size of 16Cr-0.5Hf ODS steel is significantly smaller than that of 16Cr ODS steel during the grain coarsening process of HIP.

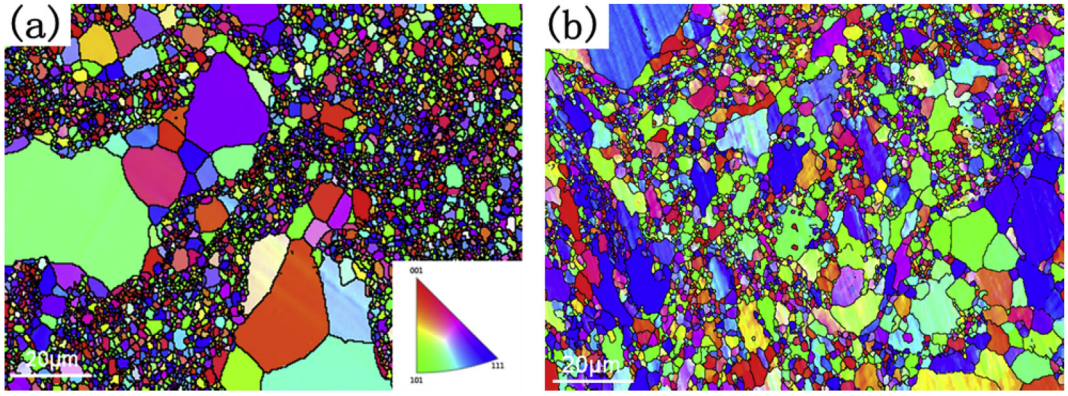

Fig. 5. EBSD grain orientation maps (inverse pole figure X, IPFX) of (a) 16Cr ODS and (b) 16Cr-0.5Hf ODS steels.

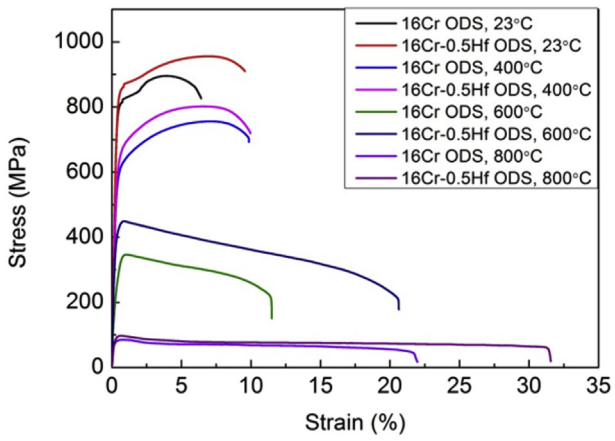

Fig. 7. Tensile curves of 16Cr ODS and 16Cr-0.5Hf ODS steels at several test temperatures (RT, 400 °C, 600 °C, 800 °C).

3.4. Tensile properties

Fig. 7 shows the tensile stress-strain curves measured at various temperatures (from RT to 800 °C) for 16Cr ODS and 16Cr-0.5Hf ODS steels. Obviously, the curves of 16Cr-0.5Hf ODS steel are higher than those of 16Cr ODS at all four test temperatures, which represents better tensile properties. It is observed a great deterioration of the mechanical properties of both alloys at 800 °C. This phenomenon is mainly due to the change of fracture mechanism from transgranular to intergranular caused by grain boundary decohesion at elevated temperatures. Grain boundaries become the weakest part of material due to the severe decrease of boundary strength at 800 °C. Cracks initialize and propagate along the grain boundaries and thus the dispersion strengthening caused by oxides cannot be well reflected. In addition, a larger degree of oxidation occurred to the samples of both alloys at 800 °C which also deteriorate the tensile performances. The tensile properties involving yield strength (YS), ultimate tensile strength (UTS) and total elongation (TE) are illustrated in Fig. 8. For a comparison purpose, the mechanical properties for a commercial ODS alloy MA956, which has similar composition to the ODS steels presented in this study, are also included [29].

As shown in Fig. 8 (a) and (b), the YS and UTS for all three steels decrease with increasing temperature. It also can be noted from Fig. 8 that both ODS steels in the present work exhibit superior tensile strengths than MA956 at all test temperatures except 800 °C. Moreover, the YS and UTS of the 16Cr-0.5Hf ODS steel are higher than those of the 16Cr ODS sample, which indicates that Hf addition can effectively improve the tensile strength for such kind of ODS steel. As shown in Fig. 8 (c), the total elongation for both samples increases with the increasing temperature and reaches 22.0% for 16Cr ODS and 31.5% for 16Cr-0.5Hf ODS steel at 800 °C,

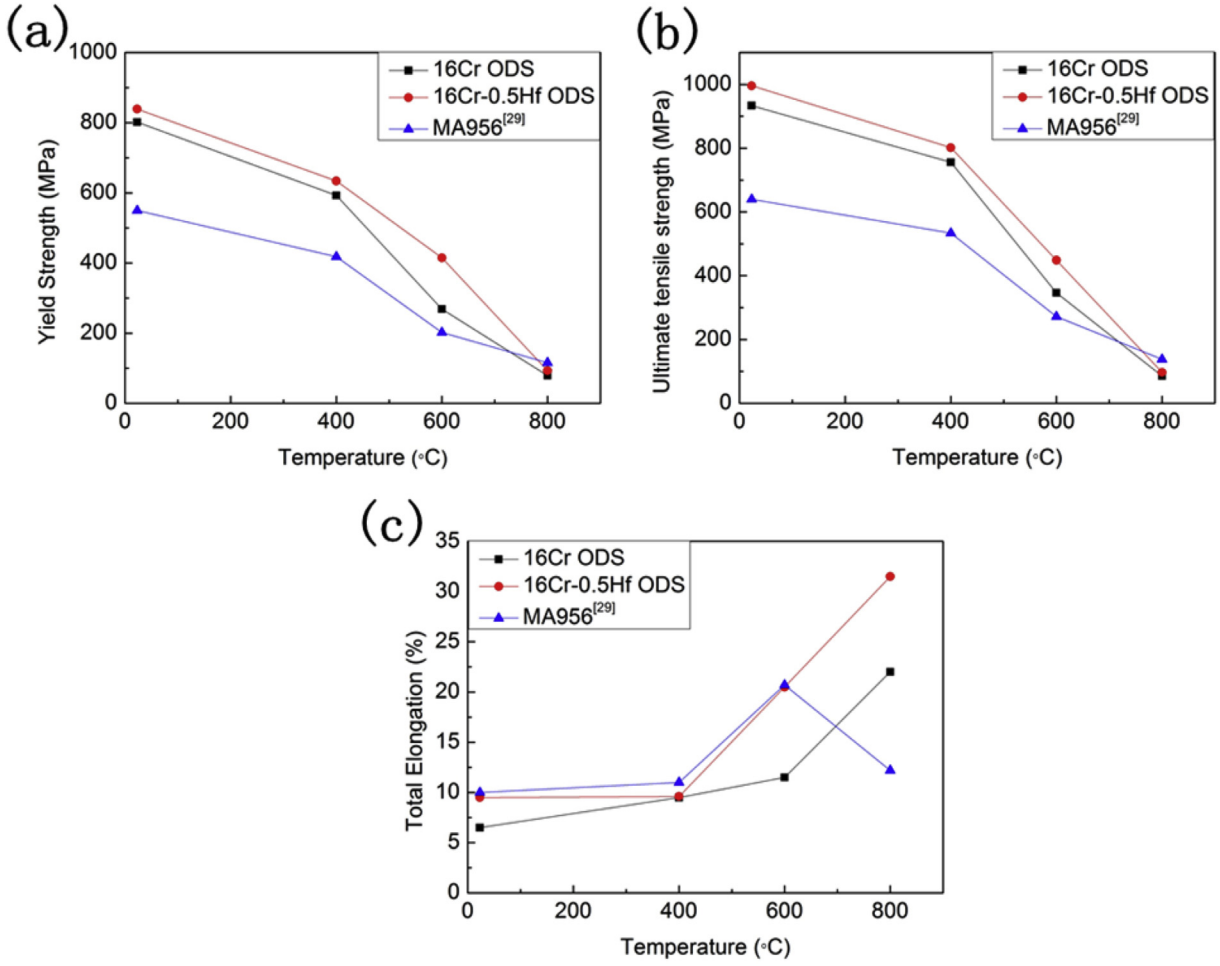

Fig. 8. Tensile properties as a function of temperature for 16Cr ODS, 16Cr-0.5Hf ODS steels and MA956 [29]: (a) Yield strength (YS), (b) Ultimate tensile strength (UTS), (c) Total elongation (TE).

respectively. It also can be noted that for MA956, the TE increases initially with an increasing temperature and reaches a significant peak at 600 °C. At the temperature below 600 °C, the 16Cr-0.5Hf ODS sample exhibits a similar TE to MA956. At 800 °C, it shows a higher TE performance than MA956, reflecting its better high temperature ductility. In generally, the ductility of the ODS steel with Hf addition is higher than 16Cr ODS steel. Therefore, the addition of Hf element can improve not only the strength but also the ductility of ODS steel.

The improvement in tensile properties observed should be attributed to the optimization in the microstructure of ODS steels. Such reinforcement effects can be explained on the basis of the combination of dispersion strengthening ($\Delta\sigma_{Orowan}$) and grain boundary strengthening ($\sigma_{H\text{-}P}$) [30]. According to Orowan pattern, the presence of finely dispersed oxide particles can act as obstacles to hinder the movement of dislocations during deformation and thus improving the mechanical strength. The strength improved by dispersed particles $\Delta\sigma_{Orowan}$ can be described as the equation [31]:

$$\Delta\sigma_{Orowan} = \frac{0.13G_m b}{\lambda}\ln\frac{d_p}{2b} \quad (2)$$

where G_m is the shear modulus for ferrite (80 GPa), b is the Burgers vector of matrix (0.248 nm), d_p is the average diameter of particles, and λ is the mean inter-particle distance of dispersed particles in matrix. As mentioned in section 3.2 and 3.3, the addition of Hf to 16Cr ODS steel can further refine the dispersed oxide particles and increase the number density. Large amounts of fine particles dispersed in the matrix provide greater resistance to the dislocation movement during the deformation process. The theoretical strength increments between $\Delta\sigma_{Orowan}$ (16Cr ODS) and $\Delta\sigma_{Orowan}$ (16Cr-0.5Hf ODS), i.e. the incremental dispersion strengthening effect of the Hf addition, calculated by Eq. (2) is 202 MPa, which clearly indicates that adding Hf would greatly enhance the yield strength of 16Cr ODS steel.

In addition, the yield strength can also be affected by the presence of grain boundaries. In accordance with Hall-Petch model, the yield strength is inversely proportional to the grain size as shown in Eq. (3):

$$\sigma_{H-P} = \sigma_0 + Kd^{-1/2} \quad (3)$$

where $\sigma_{H\text{-}P}$ is the yield strength, σ_0 is the single crystal yield strength for ferrite (30 MPa), d is the average grain size and K is a constant (0.274 MPa $\mu m^{1/2}$). The grain refinement results in the increase of strength and ductility simultaneously. Based on calculations from Eq. (3), the theoretical strength related to grain boundaries are 234 MPa ($\sigma_{16Cr\ ODS}$) and 300 MPa ($\sigma_{16Cr\text{-}0.5Hf\ ODS}$). However, the actual strength increments are much lower than the theoretical values calculated from $\Delta\sigma_{Orowan}$ and $\sigma_{H\text{-}P}$. This error may be due to the existence of pores and bonding defects in matrix, which prevent the embodiment of the reinforcement. As shown in the section “Experimental”, the relative density of 16Cr ODS sample is 98.6%, while the relative density of ODS sample with Hf is 96.1%. Much more pores can be regarded exist in 16Cr-0.5Hf ODS than 16Cr ODS steel which lower the strength of samples, therefore, the actual strengthening caused by Hf addition cannot be accurately reflected. And this may be a common problem for powder metallurgy materials. On the other hand, the inter-particle distance measurement and the statistics of particle number densities were based on the micro 2-dimensional planes, while the tensile tests showed the results of the macro 3-dimensional level. Artificial statistical errors can also affect the accuracy of the results. Although error exists between theoretical calculation and experimental measurement, the increasing trend of tensile strength with Hf addition is indisputable.

4. Conclusions

The effect of Hf element addition on the microstructure and tensile properties of 16Cr ODS steel has been investigated. Based on the results presented above, the following conclusions can be summarized:

(1) The average size of the precipitated oxide particles is significantly smaller and the number density is higher with Hf addition than that of the original 16Cr ODS steel. Meanwhile, the grain size of matrix also decreases with the increase in the refinement of the oxide particles.
(2) The addition of Hf element can suppress the formation of Y–Al–O particles by forming more stable $Y_2Hf_2O_7$ particles. The dispersed particles in 16Cr-0.5Hf ODS steel are the mixture of Y–Al–O and Y–Hf–O phases.
(3) Due to the formation of much finer oxide particles and the grain refinement of the matrix as well, adding Hf element can effectively improve the mechanical performances of Al added ODS steels including yield strength, ultimate tensile strength and ductility.

Acknowledgments

The authors are grateful to the the International Thermonuclear Experimental Reactor (ITER) Program Special Project (No. 2014GB125006 and 2015GB107003), China National Funds for Distinguished Young Scientists (No. 51325401), the National Nature Science Foundation of China (No. 51474155 and 11672200), and Natural Science Foundation of Tianjin (No. 14JCZDJC38700) for grant and financial support.

References

[1] K. Verhiest, A. Almazouzi, N. De Wispelaere, R. Petrov, Development of oxides dispersion strengthened steels for high temperature nuclear reactor applications, J. Nucl. Mater. 385 (2009) 308–311.
[2] Y. de Carlan, J.L. Bechade, P. Dubuisson, J.–L. Seran, CEA developments of new ferritic ODS alloys for nuclear applications, J. Nucl. Mater. 386–388 (2009) 430–432.
[3] S. Ukai, M. Harada, H. Okada, M. Inoue, Tube manufacturing and mechanical properties of oxide dispersion strengthened ferritic steel, J. Nucl. Mater. 204 (1993) 74–80.
[4] T. Liu, L.B. Wang, C.X. Wang, H.L. Shen, Effect of Al content on the oxidation behavior of $Y_2Ti_2O_7$-dispersed Fe-14Cr ferritic alloys, Corros. Sci. 104 (2016) 17–25.
[5] A. Wasilkowska, M. Bartsch, U. Messerschmidt, R. Herzog, Creep mechanisms of ferritic oxide dispersion strengthened alloys, J. Mater. Process. Technol. 133 (2003) 218–224.
[6] J. Lim, H.O. Nam, I.S. Hwang, J.H. Kim, A study of early corrosion behaviors of FeCrAl alloys in liquid lead–bismuth eutectic environments, J. Nucl. Mater. 407 (2010) 205–210.
[7] S. Ohtsuka, T. Kaito, M. Inoue, T. Asayama, Effects of aluminum on high-temperature strength of 9Cr–ODS steel, J. Nucl. Mater. 386–388 (2009) 479–482.
[8] R. Gao, T. Zhang, X.P. Wang, Q.F. Fang, Effect of zirconium addition on the microstructure and mechanical properties of ODS ferritic steels containing aluminum, J. Nucl. Mater. 444 (2014) 462–468.
[9] A. Kimura, R. Kasada, N. Iwata, H. Kishimoto, Development of Al added high-Cr ODS steels for fuel cladding of next generation nuclear systems, J. Nucl. Mater. 417 (2011) 176–179.
[10] S. Takaya, T. Furukawa, G. Muller, A. Heinzel, Al-containing ODS steels with improved corrosion resistance to liquid lead–bismuth, J. Nucl. Mater. 428 (2012) 125–130.
[11] H. Oka, M. Watanabe, H. Kinoshita, T. Shibayama, In situ observation of damage structure in ODS austenitic steel during electron irradiation, J. Nucl. Mater. 417 (2011) 279–282.
[12] P. He, M. Klimenkov, R. Lindau, A. Moslang, Characterization of precipitates in nano structured 14% Cr ODS alloys for fusion application, J. Nucl. Mater. 428 (2012) 131–138.

[13] Y. Zhang, T.Y. Ouyang, D.W. Liu, J.Y. Du, 9Cr-ODS steel composite material reinforced by Ta layers, J. Alloys Compd. 682 (2016) 294–301.
[14] D. Preininger, Effect of particle morphology and microstructure on strength, work-hardening and ductility behaviour of ODS-(7–13)Cr steels, J. Nucl. Mater. 329–333 (2004) 362–368.
[15] J.H. Schneibel, M. Heilmaier, W. Blum, G. Hasemann, Temperature dependence of the strength of fine- and ultrafine-grained materials, Acta Mater. 59 (2011) 1300–1308.
[16] A. Takahashi, Z.Z. Chen, N. Ghoniem, N. Kioussis, Atomistic-continuum modeling of dislocation interaction with Y2O3 particles in iron, J. Nucl. Mater. 417 (2011) 1098–1101.
[17] M. Klimiankou, R. Lindau, A. Moslang, J. Schroder, TEM study of PM 2000 steel, Powder Metall. 48 (2005) 277–287.
[18] N. Garcia, M. Campos, J.M. Torralba, M.H. Berger, Capability of mechanical alloying and SPS technique to develop nanostructured high Cr, Al alloyed ODS steels, Mater. Sci. Technol. 30 (2014) 1676–1684.
[19] L. Zhang, S. Ukai, T. Hoshino, S. Hayashi, Y2O3 evolution and dispersion refinement in Co-base ODS alloys, Acta Mater. 57 (2009) 3671–3682.
[20] G.B. Schaffer, M.H. Loretto, R.E. Smallman, J.W. Brooks, The stability of the oxide dispersion in INCONEL alloy MA6000, Acta Metall. 37 (1989) 2551–2558.
[21] M. Klimiankou, R. Lindau, A. Moslang, HRTEM study of yttrium oxide particles in ODS steels for fusion reactor application, J. Cryst. Growth 249 (2003) 381–387.
[22] A. Yabuuchi, M. Maekawa, A. Kawasuso, Influence of oversized elements (Hf, Zr, Ti and Nb) on the thermal stability of vacancies in type 316L stainless steels, J. Nucl. Mater. 430 (2012) 190–193.
[23] J.R. Rieken, I.E. Anderson, M.J. Kramer, G.R. Odette, Reactive gas atomization processing for Fe-based ODS alloys, J. Nucl. Mater. 428 (2012) 65–75.
[24] L. Zhang, X.B. He, X.H. Qu, Y. Liu, Characteristics of complex oxides in Co based ODS alloys, Powder Metall. 56 (2013) 24–31.
[25] Y.F. Li, H. Abe, F. Li, Y. Satoh, Grain structural characterization of 9Cr–ODS steel aged at 973 K up to 10,000 h by electron backscatter diffraction, J. Nucl. Mater. 455 (2014) 568–572.
[26] I. Hilger, F. Bergner, T. Weissgarber, Bimodal grain size distribution of nanostructured ferritic ODS Fe-Cr alloys, J. Am. Ceram. Soc. (2015) 1–6.
[27] C. Casas, R. Tejedor, R. Rodriguez-Baracaldo, J.A. Benito, The effect of oxide particles on the strength and ductility of bulk iron with a bimodal grain size distribution, Mat. Sci. Eng. A 627 (2015) 205–216.
[28] T. Nishizawa, I. Ohnuma, K. Ishida, Examination of the Zener relationship between grain size and particle dispersion, Mater. Trans. 38 (1997) 950–956.
[29] R.L. Klueh, J.P. Shingledecker, R.W. Swindenman, D.T. Hoelzer, Oxide dispersion-strengthened steels: a comparison of some commercial and experimental alloys, J. Nucl. Mater. 341 (2005) 103–114.
[30] P.M. Hazzledine, Direct versus indirect dispersion hardening, Scr. Metall. Mater. 26 (1992) 57–58.
[31] Z. Zhang, D.L. Chen, Consideration of Orowan strengthening effect in particulate reinforced metal matrix nanocomposites, Scr. Mater. 54 (2006) 1321–1326.